

The mid-infrared properties and gas content of active galaxies over large look-back times

S. J. Curran^{*} and S. W. Duchesne

School of Chemical and Physical Sciences, Victoria University of Wellington, PO Box 600, Wellington 6140, New Zealand

Accepted —. Received —; in original form —

ABSTRACT

Upon an expansion of all of the searches for redshifted H I 21-cm absorption ($0.0021 \leq z \leq 5.19$), we update recent results regarding the detection of 21-cm in the non-local Universe. Specifically, we confirm that photo-ionisation of the gas is the mostly likely cause of the low detection rate at high redshift, in addition to finding that at $z \lesssim 0.1$ there may also be a decrease in the detection rate, which we suggest is due to the dilution of the absorption strength by 21-cm emission. By assuming that associated and intervening absorbers have similar cosmological mass densities, we find evidence that the spin temperature of the gas evolves with redshift, consistent with heating by ultra-violet photons. From the near-infrared ($\lambda = 3.4, 4.6$ and $12 \mu\text{m}$) colours, we see that radio galaxies become more quasar-like in their activity with increasing redshift. We also find that the non-detection of 21-cm absorption at high redshift is not likely to be due to the selection of gas-poor ellipticals, in addition to a strong correlation between the ionising photon rate and the $[3.4] - [4.6]$ colour, indicating that the UV photons arise from AGN activity. Like previous studies, we find a correlation between the detection of 21-cm absorption and the $[4.6] - [12]$ colour, which is a tracer of star-forming activity. However, this only applies at the lowest redshifts ($z \lesssim 0.1$), the range considered by the other studies.

Key words: galaxies: active – quasars: absorption lines – radio lines: galaxies – ultra violet: galaxies – infrared: galaxies – galaxies: ISM

1 INTRODUCTION

Cool, neutral gas, the reservoir for star formation throughout the Universe, is traced by the absorption of the $\lambda = 21\text{-cm}$ continuum radiation by neutral hydrogen (H I). This can be detected in either the gas in galaxies *intervening* the sight-line to a background continuum source (quasar) or by the gas *associated* with the radio galaxy or quasar itself. The conditions to which the cool gas is exposed differs in each of these cases, with the intervening absorption arising in quiescent galaxies, which may trace the star-formation history (Curran 2017a,b). The associated absorption arises within the host galaxies of active galactic nuclei (AGN) and, since the total neutral hydrogen column density, $N_{\text{H I}}$, is generally not known, the spin temperature of the gas (degenerate with the covering factor, see Curran 2012) cannot be determined, which does not allow a measure of how the fraction of cool gas evolves with redshift. There has, nevertheless, been some recent advances in understanding the nature of the neutral gas in the associated absorbers:

(i) The paucity of detection of 21-cm absorption at $z \gtrsim 1$ may be due to the optical selection of sources, leading to ultra-violet

luminosities ($L_{\text{UV}} \gtrsim 10^{23} \text{ W Hz}^{-1}$) sufficient to ionise all of the neutral gas (Curran et al. 2008; Curran & Whiting 2012).

(ii) The similar detection rate for both type-1 and type-2 AGN below $L_{\text{UV}} \sim 10^{23} \text{ W Hz}^{-1}$ indicates that the absorption does not arise predominately in the sub-pc torus (e.g. Pihlström et al. 1999; Gupta et al. 2006), but in the large-scale galactic disk (Curran & Whiting 2010).

(iii) The higher detection rate in compact objects (e.g. Vermeulen et al. 2003; Geréb et al. 2014) may be due to the fact that these “young” sources have lower UV luminosities than the extended objects (Curran & Whiting 2010; Allison et al. 2012).

(iv) The absorption strength is correlated with both the visible–near-infrared ($V - K$, Curran & Whiting 2010) and blue–near-infrared ($B - K$, Curran et al. 2017b) colours, indicating that the reddening is caused by intrinsic dust, which shields the cool, neutral gas from the ambient UV field.

(v) The anti-correlation between the strength of the absorption and the size of the radio source (e.g. Pihlström et al. 2003; Chandola et al. 2011) can be explained by the effect of geometry on the coverage of the continuum source (Curran et al. 2013a). This is also evident in the increase in detection rate with turnover frequency for the gigahertz peaked spectrum sources (Curran et al. 2017b).

^{*} Stephen.Curran@vuw.ac.nz

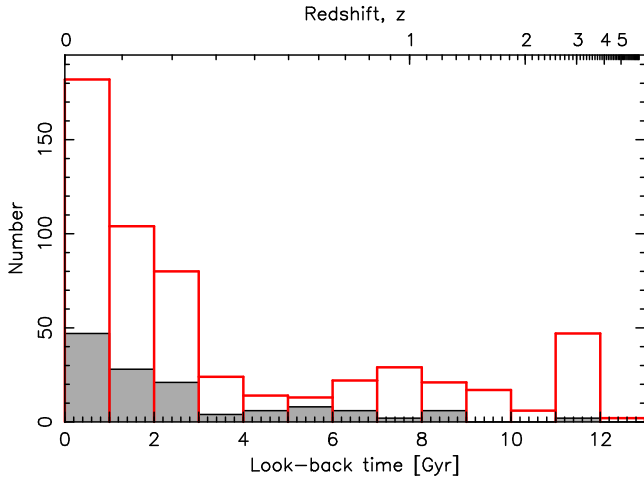


Figure 1. The distribution of the 21-cm detections (shaded histogram) and non-detections (unshaded) with look-back time. Throughout the paper we use a standard Λ cosmology with $H_0 = 71 \text{ km s}^{-1} \text{ Mpc}^{-1}$, $\Omega_{\text{matter}} = 0.27$ and $\Omega_{\Lambda} = 0.73$.

(vi) The molecular gas, detected in many instances through CO emission at $z \gtrsim 3$, is remote from the continuum source (e.g. De Breuck et al. 2003; Emonts et al. 2013), and thus not subject to the same ionising flux as the neutral gas (Curran et al. 2016a).

(vii) There is a strong relationship between 21-cm and soft X-ray absorption, each of which is consistent with the presence of dense neutral gas (Ostorero et al. 2010, 2017; Glowacki et al. 2017; Moss et al. 2017).

(viii) The detection of 21-cm absorption is related to the mid-infrared colours of the source. Specifically, a detection is more likely at a higher $4.6\text{--}12 \mu\text{m}$ colour, which is a tracer of star forming activity (Chandola & Saikia 2017; Glowacki et al. 2017).

This latter item has only been investigated at low redshift ($z \lesssim 0.2$) and, given its potential importance in future surveys for H I 21-cm absorption with the Square Kilometre Array (Morganti et al. 2015), should be expanded to include all of the redshifted 21-cm searches, which we do in this paper. Since there has been some recent discussion questioning the importance of the UV luminosity, in Sect. 2 we revisit this argument in context of the radio luminosity, which is also advocated as being a crucial factor in the detection of 21-cm absorption. In Sect. 3, we discuss the variation in the detection rate at various redshifts. In Sect. 4, we examine any correlation between the mid-infrared colours and the detection of 21-cm absorption, in addition to investigating how this is related to the ionising UV continuum. Finally, in Sect. 5 we summarise our conclusions.

2 THE EFFECT OF THE BACKGROUND CONTINUUM

2.1 The updated sample

Previously (e.g. Curran et al. 2017a), we only considered the $z \geq 0.1$ H I 21-cm absorption searches, giving 311 sources for which limits could be obtained (i.e. of sufficiently high signal-to-noise and not dominated by radio frequency interference). We now expand the sample by including all of the published redshifted searches (Fig. 1), giving a sample of 689 sources (comprising 129 detections and 560 limits), spanning redshifts of $0.0021 \leq z \leq 5.19$ (look-back times of 0.03 to 12.5 Gyr). These have been compiled from de Waard et al.

(1985); Mirabel (1989); van Gorkom et al. (1989); Uson et al. (1991); Carilli et al. (1992, 1998, 2007); Moore et al. (1999); Peck et al. (1999, 2000); Röttgering et al. (1999); Morganti et al. (2001); Ishwara-Chandra et al. (2003); Vermeulen et al. (2003); Curran et al. (2006, 2008, 2011a,b, 2013b,c, 2016a, 2017a,b); Gupta et al. (2006); Orienti et al. (2006); Kanekar et al. (2009); Emonts et al. (2010); Salter et al. (2010); Chandola et al. (2011, 2013); Allison et al. (2012, 2015); Yan et al. (2012, 2016); Geréb et al. (2015); Srianand et al. (2015); Aditya et al. (2016, 2017); Glowacki et al. (2017); Moss et al. (2017); Maccagni et al. (2017); Ostorero et al. (2017); Grasha et al. (2018)¹ and will be available in a forthcoming on-line catalogue (Moss et al., in prep).

As described in Curran et al. (2013b), we obtain the photometry of each source from the NASA/IPAC Extragalactic Database (NED), the Wide-Field Infrared Survey Explorer (WISE, Wright et al. 2010), Two Micron All Sky Survey (2MASS, Skrutskie et al. 2006) and the Galaxy Evolution Explorer (GALEX data release GR6/7)² databases, which are then shifted into the rest-frame of the source and converted to a luminosity upon correction for Galactic extinction (Schlegel et al. 1998).

2.2 Ultra-violet

From a survey for H I 21-cm absorption at high redshift, Curran et al. (2008) obtained zero detections out of the ten $z \gtrsim 3$ sources searched. Upon a detailed investigation of the source photometries, they suggested that the high redshifts introduced a selection effect, where the faint optical targets ($B \gtrsim 19$) were in fact UV bright in the source rest-frame, thus ionising/exciting the gas to below the detection limit. Although this “critical UV luminosity” of $L_{\text{UV}} \sim 10^{23} \text{ W Hz}^{-1}$ has not yet been falsified by several consequent surveys (Curran et al. 2011a, 2013b,c, 2016a, 2017a,b; Allison et al. 2012; Geréb et al. 2015; Aditya et al. 2016, 2017; Aditya & Kanekar 2018; Grasha et al. 2018), Aditya et al. (2016) and Aditya & Kanekar (2018) suggest that other effects may be responsible for the non-detections. Namely, gas excitation by the incident radio continuum or some unspecified redshift evolution.

Before addressing this, it should be noted that Aditya et al. use the $\lambda = 912 \text{ \AA}$ monochromatic luminosity (Curran et al. 2008), when in fact it is the *total* bolometric luminosity at $\lambda \leq 912 \text{ \AA}$, which should be used (Curran & Whiting 2012). The ionising photon rate, $Q_{\text{H I}} \equiv \int_{\nu}^{\infty} (L_{\nu}/h\nu) d\nu$, is obtained from a power-law fit to the extinction corrected blue/UV ($\nu \gtrsim 10^{15} \text{ Hz}$) photometry, which we show for all of the sources which have sufficient data in Fig. 2. The highest ionising photon rate at which H I has been detected ($Q_{\text{H I}} = 4.8^{+3.2}_{-1.9} \times 10^{56} \text{ sec}^{-1}$) is now due to PKS 1200+045 (Aditya & Kanekar 2018).³ This value is quite unreliable since the SED has only one value above the ionising frequency (Fig. 3) and does not include a break in the power-law.⁴ However, if we assume this to be valid, our model (Curran & Whiting 2012), which applies the equation of photoionisation equilibrium (Osterbrock 1989)

¹ Grasha et al. (2018), which is still in submission, reports 0 new detections of H I 21-cm absorption out of 89 new searches over $0.02 < z < 3.8$ (see Grasha & Darling 2011).

² <http://galex.stsci.edu/GR6/#mission>

³ From $L_{\text{UV}} \approx Q_{\text{H I}} h$, this gives a monochromatic luminosity of $L_{\text{UV}} \approx 3 \times 10^{23} \text{ W Hz}^{-1}$.

⁴ The UV continuum in Quasi-Stellar Objects (QSOs) is seen to follow a broken power law, with a break close to $\lambda = 1200 \text{ \AA}$ and spectral indices of $\alpha_{\text{NUV}} \approx -1$ and $\alpha_{\text{EUV}} \approx -2$ at $\lambda \gtrsim 1200 \text{ \AA}$ and $\lambda \lesssim 1200 \text{ \AA}$, respectively (see Shull et al. 2012 and references therein).

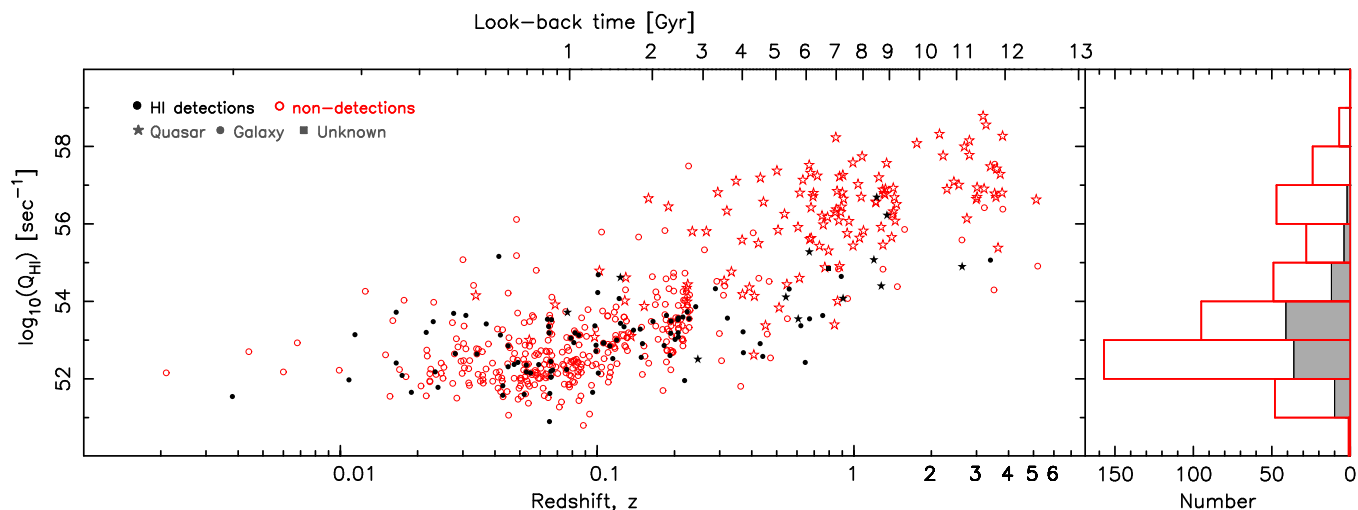


Figure 2. The ionising ($\lambda \leq 912 \text{ \AA}$) photon rate versus redshift for the H I 21-cm absorption searches. The filled circles/histogram represent the detections and the unfilled circles/histogram the non-detections, with the shapes representing the classification as given by the NASA/IPAC Extragalactic Database (NED).

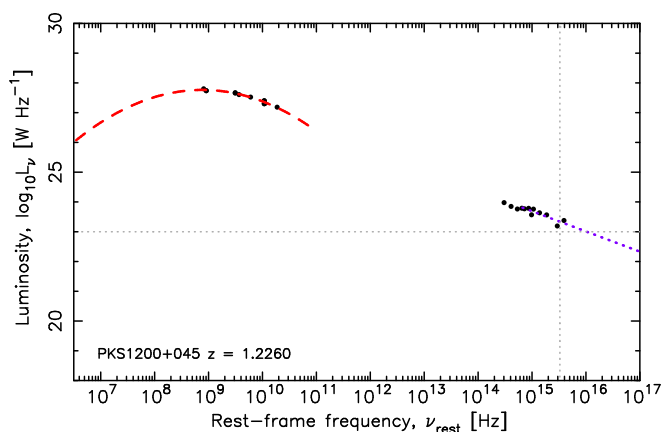


Figure 3. The available photometry of PKS 1200+045 overlaid by fits to the radio and optical/UV points (see Curran et al. 2013b). The vertical dotted line signifies a rest-frame frequency of $3.29 \times 10^{15} \text{ Hz}$ ($\lambda = 912 \text{ \AA}$) and the horizontal a $\lambda = 912 \text{ \AA}$ luminosity of $L_{UV} = 10^{23} \text{ W Hz}^{-1}$.

to an exponential gas disk, yields a scale-length of $R = 2.8 \text{ kpc}$ for $Q_{HI} = 4.8 \times 10^{56} \text{ sec}^{-1}$, using the canonical gas temperature of 2000 K, or $R = 2.1 \text{ kpc}$, using the $T = 500 \text{ K}$ typical of intervening systems (Curran et al. 2016c; Curran 2017b). This compares to 3.15 kpc for the Milky Way (Kalberla & Kerp 2009), showing that an ionising rate of $Q_{HI} = 4.8 \times 10^{56} \text{ sec}^{-1}$ is insufficient to completely ionise the gas in a large spiral, thus not requiring a re-evaluation of the critical ionising photon rate.

Of the 512 sources with sufficient UV photometry, below the highest value where 21-cm absorption has been detected there are 106 detections and 406 non-detections, giving a detection rate of 20.7%. Using a detection probability of $p = 0.207$, where $p = 0.5$ is even odds, the binomial probability of obtaining the observed zero detections out of 50 searches for 21-cm absorption is $P(\text{bin}) = 9.18 \times 10^{-6}$. Assuming Gaussian statistics, this is significant at $S(\text{bin}) = 4.42\sigma$. This is lower than the 6.83σ significance reported by Curran et al. (2017a), although only $z \geq 0.1$ sources were considered and below these redshifts there may be another factor at play which lowers the detection rate (see Sect. 3.1).

It should be noted that, while there are 48 quasars above the

critical ionising photon rate, there are only two galaxies. It is therefore tempting to attribute the lack of detection of 21-cm absorption above the critical rate to an unfavourable alignment of the continuum emission and absorbing gas along our sight-line. However, although all of the sources with $L_{UV} \gtrsim 10^{23} \text{ W Hz}^{-1}$ are type-1 AGN, for those below this there is a 50% detection rate for both type-1 and type-2 objects (Curran & Whiting 2010).⁵ Thus, the orientation of inner torus has little bearing upon the detection of 21-cm absorption, which must occur in a randomly oriented large-scale galactic disk (e.g. Nagar & Wilson 1999).⁶

There does, however, remain the possibility that in all of the $L_{UV} \gtrsim 10^{23} \text{ W Hz}^{-1}$ objects the gas simply does not occult the unobscured AGN along our sight-line. This would imply a selection effect where the higher UV flux is due to the absence of dense intervening gas, representing a sub-sample where the torus and disk are roughly aligned, thus differing from the $L_{UV} \lesssim 10^{23} \text{ W Hz}^{-1}$ type-1 objects. However, the complete ionisation of the neutral atomic gas in a large galaxy at this luminosity is consistent with the model of Curran & Whiting (2012). Furthermore, Page et al. (2012) note a critical X-ray luminosity, above which sources are not detected in 250 μm emission, which is a tracer of star formation. The fact that it is not detected in *emission* above a certain value cannot be attributed to orientation. Whether due to complete ionisation of the gas or a selection bias towards type-1 objects, where the galactic disk is coplanar with the torus, the fact remains that H I 21-cm has not been detected above $Q_{HI} \sim 5 \times 10^{56} \text{ sec}^{-1}$.

2.3 Radio

H I 21-cm absorption traces the cool component of the neutral gas and, in addition to ionisation of H I by $\lambda \leq 912 \text{ \AA}$ photons, the non-detection of 21-cm absorption can be caused by excitation to the upper hyperfine level by $\lambda = 21 \text{ cm}$ photons (Purcell & Field 1956; Bahcall & Ekers 1969). Although we have previously ruled this out

⁵ Based upon 21 type-1 and 33 type-2 objects with $L_{UV} < 10^{23} \text{ W Hz}^{-1}$. For the current sample there is a 21.8% detection rate for galaxies ($n = 428$) and 14.3% for quasars ($n = 132$) at $Q_{HI} > 4.8 \times 10^{56} \text{ sec}^{-1}$.

⁶ Although a small contribution from the torus is detected in the stacked absorption spectra (Curran et al. 2016b).

as a reason for the non-detections at high redshift (Curran et al. 2008; Curran & Whiting 2010; Curran et al. 2013c), from a sample of 52 flat-spectrum sources, Aditya et al. (2016) suggest that the radio luminosity may be as important as the UV luminosity in the detection of 21-cm absorption. Being “uniformly selected flat-spectrum sources” (although the spectral indices range $-1.2 \lesssim \alpha \lesssim 1.2$), these form a biased sub-sample of redshifted radio sources.

In Fig. 4, we show the distribution of 1.4 GHz continuum luminosities, where the highest luminosities represented by the histogram show a mix of detections and non-detections (cf. Fig. 2). In this case, the highest luminosity at which 21-cm absorption is detected is $L_{1.4 \text{ GHz}} = 4.38 \times 10^{28} \text{ W Hz}^{-1}$. Below this value there are 105 detections and 422 non-detections, giving a detection rate of 19.9%. Applying $p = 0.199$ to the sources with radio luminosities of $L_{1.4 \text{ GHz}} > 4.38 \times 10^{28} \text{ W Hz}^{-1}$, the binomial probability of zero detections out of nine searches is $P(\text{bin}) = 0.135$, which is significant at just $S(\text{bin}) = 1.49\sigma$. Thus, it is clear that the radio luminosity is not as important in the detection of 21-cm absorption and that any bias towards non-detections at high radio luminosities is probably due to the fact that these will tend also be the high UV luminosity sources (Curran & Whiting 2010).

Addressing the suggestion by Aditya et al. (2016) and Aditya & Kanekar (2018) that the non-detections at high redshift may be due to an unspecified dependence on redshift, the highest redshift detection is at $z = 3.398$ (Uson et al. 1991), below which there are 105 detections and 416 non-detections (a 20.2% detection rate). Above this redshift there are 19 non-detections, which gives a binomial probability of $P(\text{bin}) = 0.034$, which is significant at $S(\text{bin}) = 2.12\sigma$. Again, this is not as significant as the effect of the UV luminosity, although certainly degenerate with it.

Statistically, it is therefore clear that the ionisation of the neutral gas is the dominant effect in the non-detection of associated 21-cm absorption at high redshift. The value of the critical luminosity also remains consistent with the model of Curran & Whiting (2012), which shows that rates of $Q_{\text{H I}} \gtrsim 5 \times 10^{56} \text{ sec}^{-1}$ ($L_{\text{UV}} \gtrsim 3 \times 10^{23} \text{ W Hz}^{-1}$) are required to fully ionise the disk of a large spiral galaxy.

3 EVOLUTION OF THE NEUTRAL GAS

3.1 Line-strength

As mentioned in Sect. 1, there is evidence that the H I 21-cm absorption strength in intervening systems may trace the star formation history of the Universe (Curran 2017a,b). Plotting the 21-cm absorption strength versus redshift, we also see a peak for the associated systems (Fig. 5)⁷, although this is at a redshift of $z \sim 0.1$, cf. $z \sim 2.5$ for the intervening absorbers. The decrease in strength with increasing redshift can be attributed to increasing UV luminosities (Sect. 2.2), at least at $z \gtrsim 0.1$, where there is a 3.66σ anti-correlation between $N_{\text{H I}} f / T_{\text{spin}}$ and $Q_{\text{H I}}$ (Curran et al. 2017b). Below $z \sim 0.1$, however, the cause is not clear, although the numbers are small (at least at $z \lesssim 0.05$, Fig. 5, bottom panel). A likely

possibility is that at these redshifts 21-cm emission becomes more detectable and the decrease in the absorption line strength may be due to dilution by 21-cm emission (e.g. Reeves et al. 2015).

3.2 Spin temperature

When combined with the total neutral hydrogen column density, $N_{\text{H I}}$, the spin temperature, T_{spin} , degenerate with the covering factor f , may be estimated. Assuming that the Lyman- α absorption, which yields $N_{\text{H I}} [\text{cm}^{-2}]$, and the 21-cm absorption arise in the same sight-line, in the optically thin case (when the observed optical depth is $\tau_{\text{obs}} \lesssim 0.3$), $T_{\text{spin}} [\text{K}]$ is given by (Wolfe & Burbidge 1975)

$$\frac{T_{\text{spin}}}{f} = \frac{N_{\text{H I}}}{1.823 \times 10^{18} \int \tau_{\text{obs}} dv},$$

where $\int \tau_{\text{obs}} dv [\text{km s}^{-1}]$ is the observed velocity integrated optical depth of the 21-cm absorption. For the associated absorbers, the column densities are generally not available but, using the method of Curran (2017b), if we assume that the associated absorbers follow the same evolution of the cosmological mass density as the intervening absorbers, then from $\Omega_{\text{H I}} = 4.0 \times 10^{-4} (z_{\text{abs}} + 1)^{0.60}$ (Crighton et al. 2017) and the redshift number density of damped Lyman- α absorption systems $n_{\text{DLA}} = 0.027(z + 1)^{1.682}$ (Rao et al. 2017)

$$\langle N_{\text{H I}} \rangle = 0.011(z + 1)^{0.92} \frac{3 H_0^2}{8 \pi G} \frac{c}{m_{\text{H}} H_z},$$

where G is the gravitational constant, c is the speed of light, m_{H} is the mass of the hydrogen atom and H_z is the Hubble parameter at redshift z .

Applying the derived $\langle N_{\text{H I}} \rangle - z$ relation to the associated absorbers, gives the distribution shown in Fig. 6, where we essentially see an inverted version of the line strength distribution (Fig. 5), due to the generally flat evolution of $\langle N_{\text{H I}} \rangle$. As per the intervening absorbers, the degeneracy with the covering factor is difficult to break, although, since the absorption occurs at the same redshift as the continuum emission, there will be no bias due to the absorber and emitter being at different angular diameter distances (Curran & Webb 2006). Since the covering factor can have a value $\tau_{\text{obs}} < f \lesssim 1$ (O’Dea et al. 1994), the values in Fig. 6 represent lower limits to the spin temperature for all of the measurements.

If we take this at face value, however, there is an apparent increase in the spin temperature with redshift, which may be expected from the selection of more UV luminous sources. The lowest value for which $Q_{\text{H I}} > 4.8 \times 10^{56} \text{ sec}^{-1}$ is $T_{\text{spin}}/f \gtrsim 30 \text{ K}$, not a particularly tight constraint, or even applicable, given that we expect complete ionisation of the neutral gas. On the other hand, the highest value at which 21-cm absorption has been detected is $T_{\text{spin}}/f = 8270 \text{ K}$, similar to that of the intervening absorbers (Curran 2017a).

4 WISE COLOURS

4.1 Redshift evolution

The mid-infrared colours can provide insight into the activity within a source (Wright et al. 2010), specifically the bands observed by the Wide-Field Infrared Survey Explorer, where the $\lambda = 3.4 \mu\text{m}$ (WISE W1) and $4.6 \mu\text{m}$ (WISE W2) bands trace hot dust in the sub-pc torus (by AGN activity) and the $12 \mu\text{m}$ (WISE

⁷ As described in Curran et al. (2017a), all of the limits are re-sampled to the same spectral resolution of 20 km s^{-1} . For the binning in the middle panel, the upper limits are included as censored data points, via the *Astronomy SURVival Analysis* (ASURV) package (Isobe et al. 1986). The points are binned via the Kaplan–Meier estimator, giving the maximum-likelihood estimate based upon the parent population (Feigelson & Nelson 1985).

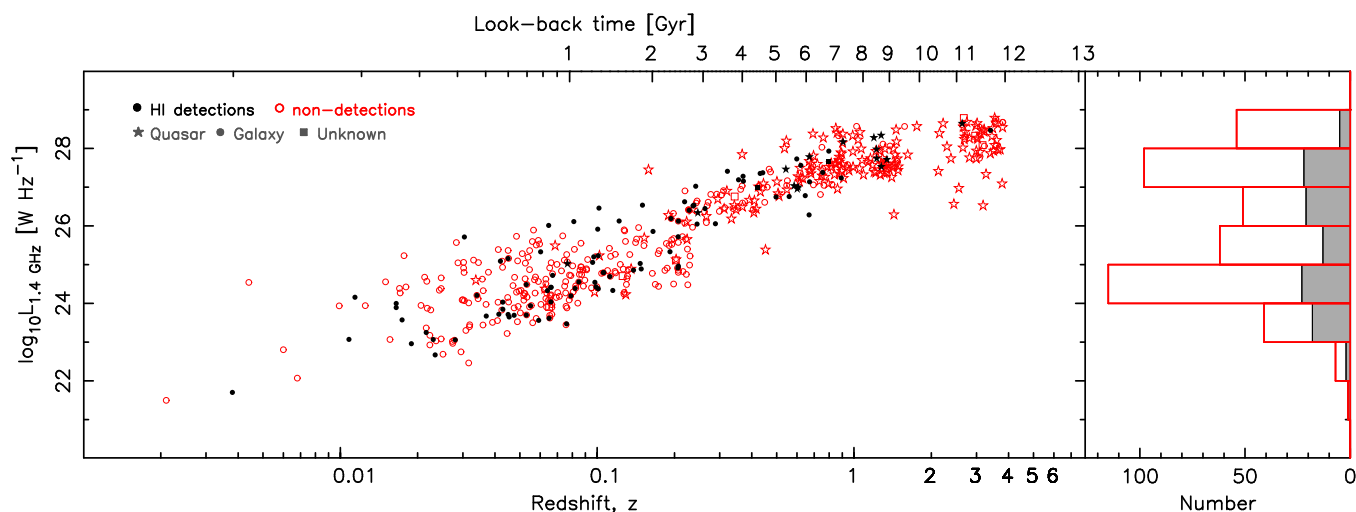


Figure 4. The rest-frame 1.4 GHz continuum luminosity versus redshift for the H I 21-cm absorption searches. As per Fig. 2, the filled symbols/histogram represent the detections and the unfilled symbols/histogram the non-detections.

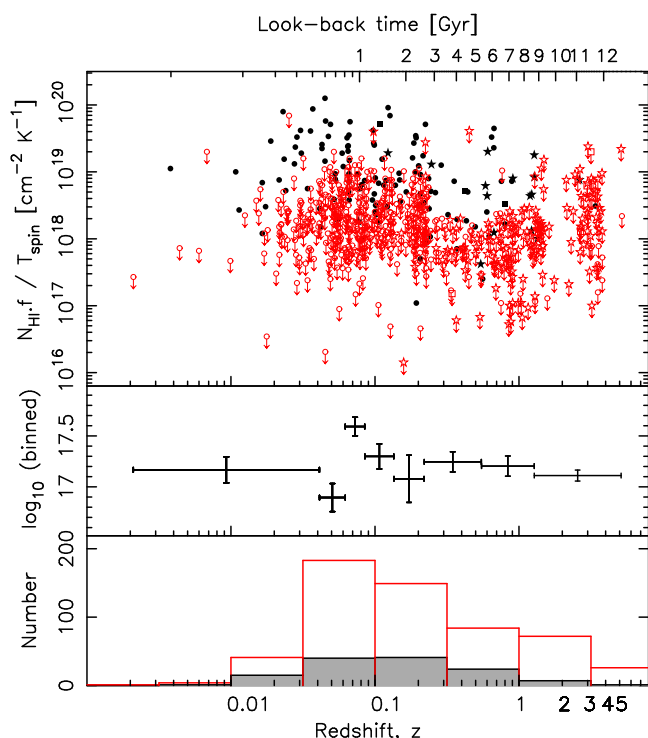


Figure 5. The line strength ($1.823 \times 10^{18} \int \tau_{\text{obs}} dv$) versus redshift for the associated H I 21-cm absorption searches. The filled symbols/histogram represent the detections and the unfilled symbols/histogram the 3σ upper limits to the non-detections. The middle panel shows the binned values in equally sized bins, including the limits. The horizontal error bars show the range of points in the bin and the vertical error bars the error in the mean value. In the bottom panel the filled histogram shows the number of detections and the unfilled the non-detections.

W3) band traces the dust heated in the host galaxy (Jarrett et al. 2011; Donoso et al. 2012). In Fig. 7, we show the observed-frame WISE colours for the sources searched in H I 21-cm absorption, where available. From this, we see a separation between the galaxies and quasars as expected from their WISE colours (Wright et al. 2010), although the (radio) galaxies have elevated [3.4] – [4.6]

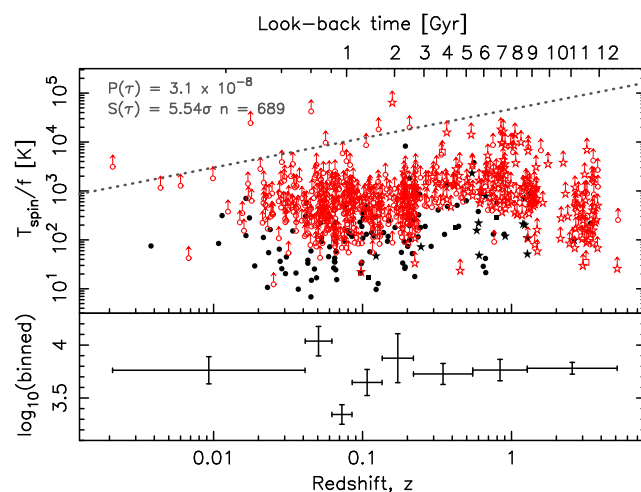


Figure 6. The estimated spin temperature (degenerate with the covering factor) for the associated 21-cm absorption searches. $P(\tau)$ shows the probability of the correlation arising by chance and $S(\tau)$ the associated significance, from a generalised non-parametric Kendall-tau test. The dotted line shows the linear regression by the Buckley–James method within the ASURV package, which includes the lower limits. The symbols and error bars in the top and bottom panels, respectively, are as per Fig. 5.

(WISE W1–W2) colours in relation to the expected distribution of spirals.

Since the sources span a large range of redshifts, $0 \lesssim z \lesssim 5$, cf. $z < 0.10$ by Glowacki et al. (2017) and $z < 0.23$ by Chandola & Saikia (2017), like Cluver et al. (2014), we also show the colours where the infrared magnitudes have been obtained from the rest-frame SED (Fig. 8). In addition to this, in Figs. 9 and 10 we split the sample into low ($z < 0.5$) and high ($z \geq 0.5$) redshift bins. The low redshift sample shows a similar distribution to the previous studies (Chandola & Saikia 2017; Glowacki et al. 2017), with the mean galaxy colour overlapping, although off-centred, to that expected for spirals (Wright et al. 2010). For the high redshift sample, however, both classes move up in [4.6] – [12], indicating more vigorous star formation. In addition to this, the galaxies move up significantly in [3.4] – [4.6], becoming more “quasar-like”.

To better illustrate these changes, in Fig. 11 we show how the

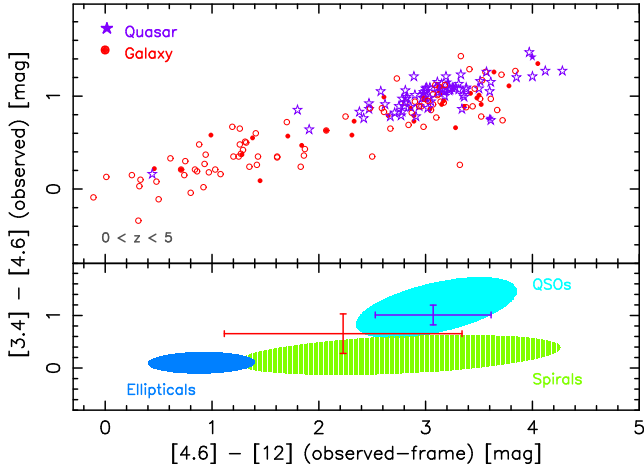


Figure 7. The observed-frame WISE colours for the sample, where available. Again, the filled symbols indicate 21-cm detections and the unfilled symbols non-detections, with the shapes representing the classification (stars–quasars, circles–galaxies, squares–unknown). The bottom panel shows the binned values, where the error bars show $\pm 1\sigma$ and the overlays show the colours of object classes (Wright et al. 2010; Glowacki et al. 2017).

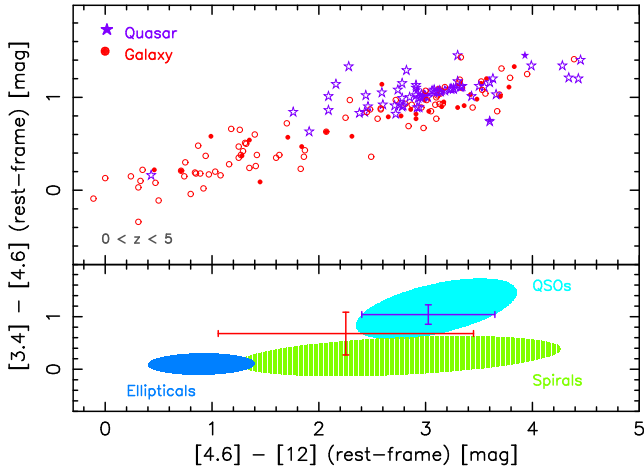


Figure 8. As Fig. 7, but in the rest-frame of the source.

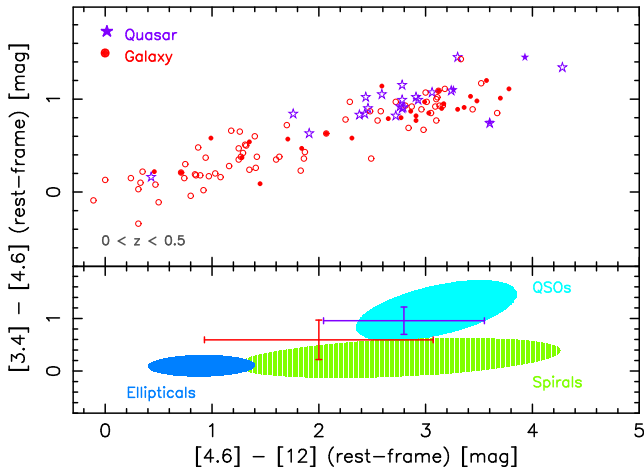


Figure 9. As Fig. 8, but for $z < 0.5$ sources only.

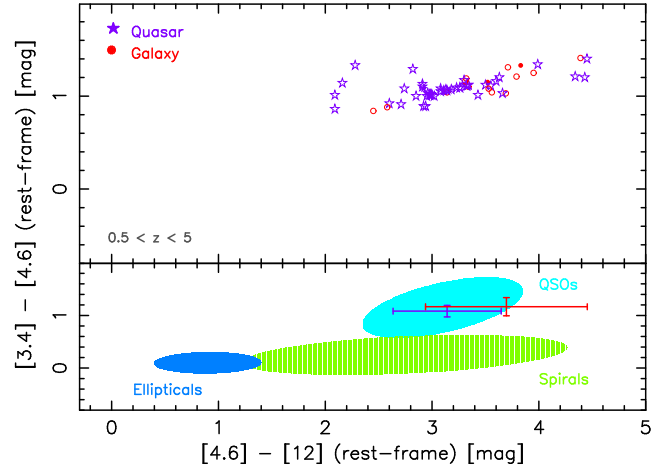


Figure 10. As Fig. 8, but for $z \geq 0.5$ sources only.

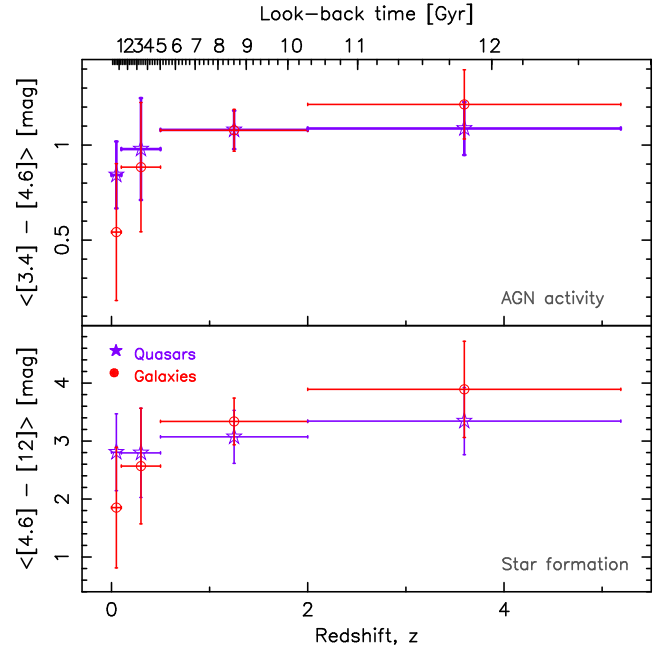


Figure 11. The WISE colours versus redshift. The vertical error bars show $\pm 1\sigma$ in the mean value and the horizontal error bars show the range of points.

colours of both classes evolve with redshift, from which we see that galaxies may increase both their star forming and AGN activity more rapidly than the quasars, although the classes are consistent to within 1σ . A possible explanation is that only the brightest objects are detected at high redshift. Although this constitutes a possible selection effect, it does tell us that previous searches for high redshift 21-cm absorption, which rely upon an optical redshift, are biased towards different objects than at low redshift (Sect. 2.2).

Finally, the redshift evolution of the colours indicates that the morphologies of high redshift galaxies searched for 21-cm absorption are unlikely to be dominated by ellipticals (Fig. 10). This is consistent with the hypothesis of Curran & Whiting (2010), that photo-ionisation, rather than a selection bias towards these gas-poor galaxies, is the cause of the low detection rates.

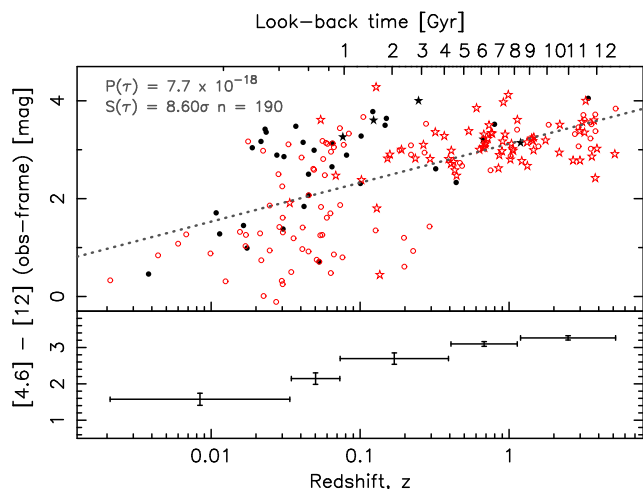


Figure 12. The $[4.6] - [12]$ observed-frame colour versus redshift. $P(\tau)$ shows the probability of the correlation arising by chance and $S(\tau)$ the associated significance, from a generalised non-parametric Kendall-tau test. The dotted line shows the best fit (see Table 1). As previously, the filled symbols represent the 21-cm detections and the unfilled symbols the non-detections, with the shapes representing the classification (stars–quasars, circles–galaxies, squares–unknown).

4.2 Colour– z relations

From the above colour dependences on redshift, it is possible that the WISE colours may provide an estimate of a redshift where an optical spectrum is not available or desired. For example, as a means of estimating redshifts for the large number of sources expected to be detected through forthcoming radio continuum surveys (e.g. the Evolutionary Map of the Universe, Norris et al. 2011), which would otherwise be observationally expensive. Also, in the search for high redshift atomic and molecular gas in absorption, where optical brightness can select against a detection (Curran et al. 2008 & Curran et al. 2011, respectively, see Sect. 2.2).

A correlation between the $\lambda = 2.2 \mu\text{m}$ K -band magnitude and redshift is well documented (Lilly & Longair 1982; Eales et al. 1997; Jarvis et al. 2001; De Breuck et al. 2002; Willott et al. 2003; Inskip et al. 2010), as well as for the near-by $3.4 \mu\text{m}$ (WISE W1) band (Collier et al. 2014; Glowacki et al. 2018). In Figs. 12 and 13 we show the $[4.6] - [12]$ and $[3.4] - [4.6]$ colours versus redshift, which are very strongly correlated [$S(\tau) = 8.60\sigma$ and 17.69σ , respectively]. The stronger correlation for the $[3.4] - [4.6]$ colour could be due to the larger sample and so, in order to compare the correlations on an equal footing, we perform a Monte Carlo simulation with 10 000 trials, where for each we select 190 $[3.4] - [4.6] - z$ pairs at random from the 619 available. Showing the results in Fig. 14, it does appear possible that the $[4.6] - [12] - z$ correlation may be just as significant.

We can compare each parameter’s effectiveness as a redshift estimator via machine learning techniques, using parameters which do not rely upon knowing the redshift of the source. We select the observed 1.4 GHz flux, S_{obs} , the radio-band turnover frequency, ν_{TO} , the radio-band spectral index, α , and the blue and mid-infrared magnitudes/colours as the *features* for the WEKA package (Hall et al. 2009). We create several classes by dividing the redshift space into $\Delta \log_{10}(z + 1) = 0.1$ bins, from which we obtain an accuracy of 68.5 – 71.4% (depending upon the algorithm, see Curran et al. 2016b) in predicting the correct class. In Table 1,

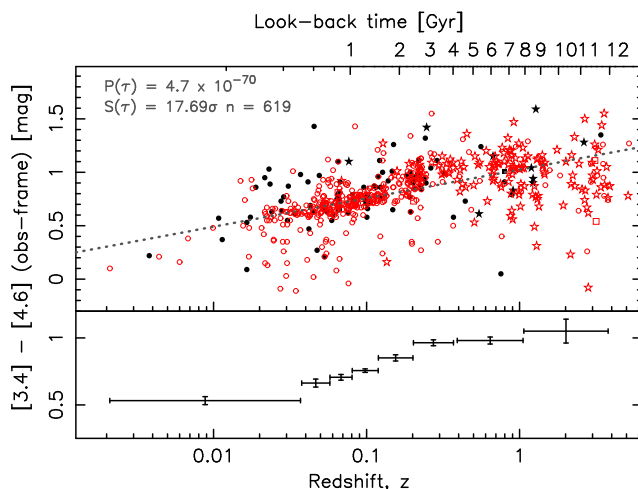


Figure 13. As Fig. 12, but for the $[3.4] - [4.6]$ colour.

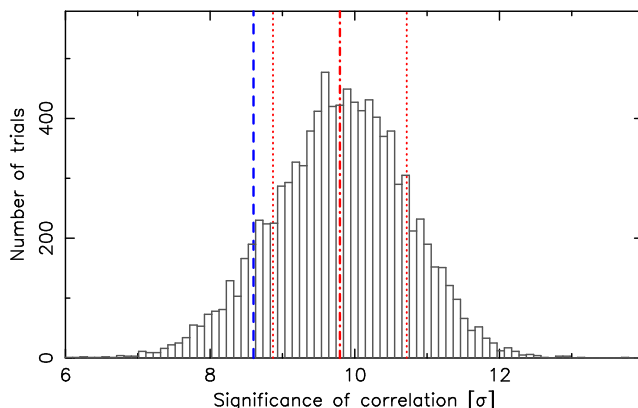


Figure 14. The distribution of the significance of the correlation for 10 000 trials of 190 $[3.4] - [4.6] - z$ pairs (Fig. 13). The dot-dashed line shows the mean ($\mu = 9.794$) and the dotted lines the standard deviation ($\sigma = 0.924$) from this. The dashed line shows the significance of the $[4.6] - [12] - z$ correlation (Fig. 12).

we summarise the significance and fits of the features in order of descending ranking. This confirms the finding of Glowacki et al. (2018) that the $3.4 \mu\text{m}$ and $4.6 \mu\text{m}$ magnitudes are more effective than most other indicators, although, not surprisingly, similar to the K -band ($2.2 \mu\text{m}$) effectiveness. All values, however, have a low correlation coefficient $|r| \ll 1$, with the WISE colours not being highly ranked, although the redshift fit could be “tighter” than from other features, since the uncertainties in the fitted slope are similar to that of the near-infrared magnitudes ($\Delta m/m \leq 0.1$) and so these may be the key to the prediction of a statistical redshift: While significant correlations between the radio spectral index and redshift have previously been noted (e.g. Athreya & Kapahi 1998; De Breuck et al. 2002), the scatter is generally too large to permit a useful prediction (Majic 2015).

4.3 H I detection

Although not seen in their own sample of compact ($\theta_{20 \text{ GHz}} < 15$ arcsec) radio sources, Glowacki et al. (2017) note that all of the flux selected ($S_{1.4 \text{ GHz}} > 50 \text{ mJy}$) sources of Geréb et al. (2015), with WISE colours of $[4.6] - [12] > 2.7$, are detected in 21-cm absorption. Furthermore, Chandola & Saikia (2017) note a high detection

Table 1. Parameter fits to $\log_{10} z$ in order of decreasing importance, given by the Pearson's correlation coefficient, r , for $\Delta \log_{10}(z + 1) = 0.1$ wide classes, using the Random Forest algorithm (Hall et al. 2009). The magnitudes and colours are in the observed frame. $P(\tau)$ gives the probability of the correlation arising by chance, from a generalised non-parametric Kendall-tau test, and $S(\tau)$ the associated significance. Note that, for the sake of comparison, for the fluxes and magnitudes we assume the null hypothesis that these are independent of redshift. The gradient and intercept are obtained via linear regression by the Buckley–James method.

Feature	n	r	$P(\tau)$	$S(\tau)$	Gradient, m	$\Delta m/m$	σ_m	Intercept
$\log_{10} S_{\text{obs}}$	686	0.3177	0.0675	1.83σ	-0.034 ± 0.063	1.85	1.05	0.16
$3.4 \mu\text{m mag}$	618	0.1889	≈ 0	23.08σ	2.194 ± 0.084	0.04	1.31	13.92
$4.6 \mu\text{m mag}$	618	0.1706	≈ 0	20.88σ	2.017 ± 0.082	0.04	1.28	13.02
K magnitude	510	0.1667	≈ 0	24.23σ	2.604 ± 0.070	0.03	0.97	14.98
B magnitude	565	0.1368	7.21×10^{-90}	20.01σ	1.775 ± 0.251	0.14	3.82	18.85
$[3.4] - [4.6]$	619	0.1200	4.75×10^{-70}	17.69σ	0.267 ± 0.022	0.08	0.34	1.03
$B - K$	572	0.0600	2.10×10^{-5}	4.25σ	-0.469 ± 0.076	0.16	1.08	4.54
Spectral index, α	576	0.0450	3.36×10^{-9}	5.91σ	0.185 ± 0.038	0.21	0.62	-0.20
$12 \mu\text{m mag}$	190	0.0361	7.94×10^{-16}	8.06σ	1.76 ± 0.18	0.10	1.97	10.15
$[4.6] - [12]$	190	0.0195	7.69×10^{-18}	8.60σ	0.796 ± 0.073	0.09	0.80	3.12
ν_{TO}	TO	0	0.049	1.97σ	0.221 ± 0.111	0.50	0.95	9.71
	All [†]	369	—	1.76σ	0.372 ± 0.111	0.30	0.95	8.54

[†] Assumes that where a turnover in the radio SED has not been detected that ν_{TO} is located below the lowest observed frequency and so is included as an upper limit (see Curran et al. 2017b). The previous row is for where a turnover is detected only, which, unlike the limits, can be readily input to WEKA.

Table 2. The $[4.6] - [12]$ (WISE W2–W3) H I 21-cm detection statistics for n values within the redshift range. The third column gives the median $[4.6] - [12]$ colour of the quoted redshift range (Fig. 11), followed by the detection rate statistics below and above this. The last two columns give the binomial probability and significance of this observed number of detections or more at $[4.6] - [12] \geq$ the median, given the detection rate below the median value.

z -range	n	Median	Rate [%]		$P(\text{bin})$	$S(\text{bin})$
		Below	Above			
All	173	2.82	16.3	25.3	0.021	2.31σ
< 0.1	82	1.84	17.1	39.0	7.04×10^{-4}	3.39σ
$0.1 - 0.5$	39	2.78	17.6	27.3	0.179	1.34σ
$0.5 - 2$	36	3.11	5.6	11.1	0.264	1.12σ
$2 - 5$	15	3.55	0	12.5	—	—

rate (70%) in compact objects with $[4.6] - [12] > 2.0$. Since, for the whole sample, the $[4.6] - [12]$ values increase with redshift (Sect. 4.1), we examine the binomial probability of the number of detections or more about the median value (Table 2), which exceeds 2.7 above $z = 0.5$ (Fig. 10). From the table, we only see a correlation at the lowest redshifts which is consistent with that found for $z \leq 0.23$ sources by Chandola & Saikia (2017) and in the Geréb et al. (2015) data.

Glowacki et al. (2017) suggest that there is also an anti-correlation between the $[3.4] - [4.6]$ colour and the 21-cm detection rate, which could be consistent with excitation of the neutral gas by the AGN (Sect. 2). However, any such correlation is weak (Table 3).

4.4 Photo-ionisation

Although the AGN activity, as traced through the $[3.4] - [4.6]$ colour, appears to have little effect on the 21-cm detection rate (Table 3), we know that the UV luminosity does. From the ionising photon rate versus the $[3.4] - [4.6]$ colour (Fig. 15), we find a very

Table 3. As Table 2, but for the $[3.4] - [4.6]$ (WISE W1–W2) colours.

z -range	n	Median	Rate [%]		$P(\text{bin})$	$S(\text{bin})$
			Below	Above		
All	526	0.75	16.1	20.2	0.056	1.91σ
< 0.1	273	0.67	17.6	19.7	0.280	1.08σ
$0.1 - 0.5$	196	0.88	18.4	23.5	0.122	1.55σ
$0.5 - 2$	39	1.07	5.3	10.0	0.284	1.07σ
$2 - 5$		1.16	0	11.1	—	—

strong correlation [$S(\tau) = 13.84\sigma$]. Of course, it is possible that some of the UV flux is due to the presence of young stars (see Curran et al. 2016a), and so we also consider the relation between the $[4.6] - [12]$ colours (Fig. 16). Although significant, this does not appear to be as strongly correlated as the $[3.4] - [4.6]$ colour. However, this only consists of 165 sources for which both $[4.6] - [12]$ and $Q_{\text{H I}}$ can be obtained, cf. 486 sources for $[3.4] - [4.6]$. Therefore, as in Sect. 4.2, we compare the correlations by selecting 165 $Q_{\text{H I}} - [3.4] - [4.6]$ pairs at random from the 486 available, the results of which are shown in Fig. 17. From this, it is clear that the $Q_{\text{H I}} - [3.4] - [4.6]$ correlation is stronger than that of $Q_{\text{H I}} - [4.6] - [12]$, suggesting a dominant AGN contribution to the UV flux.

5 SUMMARY

Upon updating the redshifted H I 21-cm absorption catalogue with the addition of $z \lesssim 0.1$ sources, we revisit the effects of the radio and ultra-violet luminosities, as well as investigating the effects of the mid-infrared colours, on the detection of cool, neutral gas in the distant Universe. We find:

- (i) For the ultra-violet and radio luminosities:
 - (a) That the ionising photon rate remains the dominant factor,

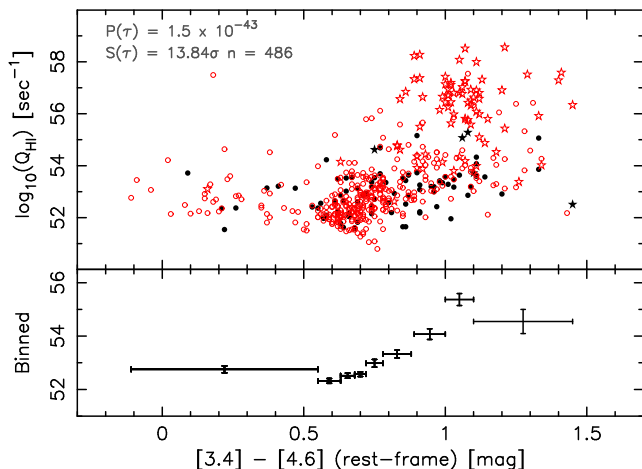


Figure 15. The ionising ($\lambda \leq 912 \text{ \AA}$) photon rate versus the rest-frame $[3.4] - [4.6]$ colour. As above, the filled symbols represent the 21-cm detections and the unfilled symbols the non-detections, with the shapes representing the classification (stars—quasars, circles—galaxies, squares—unknown). The error bars are as per Fig. 5.

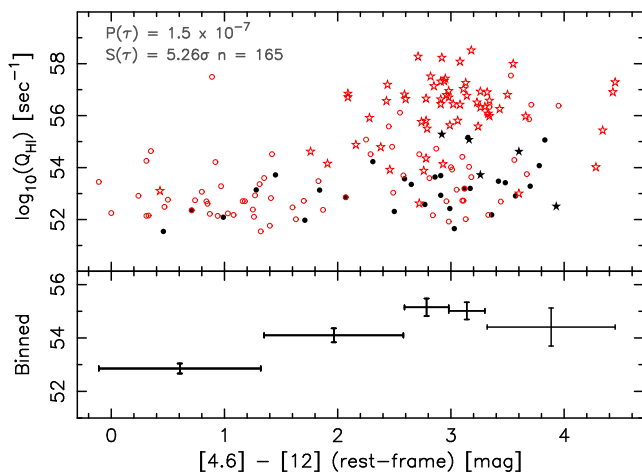


Figure 16. As per Fig. 15, but for the rest-frame $[4.6] - [12]$ colour.

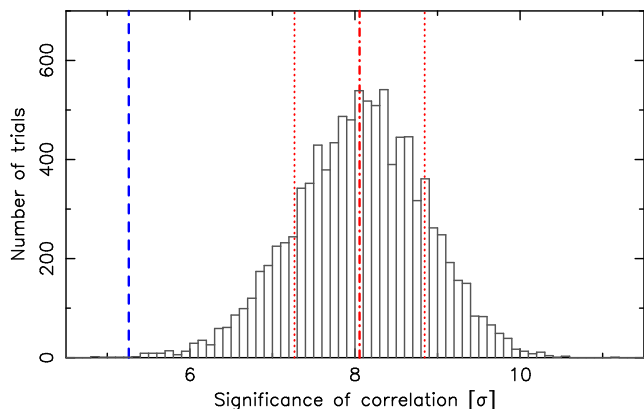


Figure 17. The distribution of the significance of the correlation for 10 000 trials of 165 $Q_{\text{HI}}-[3.4] - [4.6]$ pairs. The dot-dashed line shows the mean ($\mu = 8.056$) and the dotted lines the standard deviation ($\sigma = 0.788$) from this. The dashed line shows the significance of the $Q_{\text{HI}}-[4.6] - [12]$ correlation (Fig. 16).

over and above radio luminosity and redshift, in the detection of 21-cm absorption in the host galaxy.

(b) The highest ionising photon rate at which 21-cm absorption has been detected may be $Q_{\text{HI}} = 5 \times 10^{56} \text{ sec}^{-1}$ ($L_{\text{UV}} \approx 3 \times 10^{23} \text{ W Hz}^{-1}$). This is barely sufficient to completely ionise the gas in the large spiral, remaining consistent with the model of Curran & Whiting (2012).

(c) While the increase in ultra-violet luminosity is responsible for a decreasing 21-cm detection rate at $z \gtrsim 0.1$ (Curran & Whiting 2010), we also note a decrease at low redshift. We suggest that this is due to increased “contamination” by 21-cm emission, which strengthens with decreasing redshift, thus diluting the absorption strength.

(ii) For the mid-infrared colours:

(a) While the $[4.6] - [12]$ colours increase for both quasars and galaxies with redshift, the increase in $[3.4] - [4.6]$ colour is more pronounced for galaxies. Both increases can be attributed to the detection of only the brightest objects as the redshift increases, although the relative AGN contribution in the high redshift galaxies is larger than at low redshift. This will introduce a bias to optically selected HI 21-cm absorption searches in high redshift radio galaxies.

(b) Thus, the colours may be used to predict the source redshift, although the correlations are not as strong as for the $\lambda = 3.4$ and $4.6 \text{ }\mu\text{m}$ (Collier et al. 2014; Glowacki et al. 2018) nor the K -band ($\lambda = 2.2 \text{ }\mu\text{m}$) magnitudes (e.g. Lilly & Longair 1982; De Breuck et al. 2002).

(c) The high redshift sources searched in 21-cm absorption are unlikely to be ellipticals. A possible bias towards the selection of these gas-poor objects could offer an alternative explanation to the photo-ionisation being responsible for the lack of detections at high redshift. The WISE colours suggest that this is not the case.

(d) Both the $[3.4] - [4.6]$ and $[4.6] - [12]$ colours are correlated with the ionising photon rate, although this is stronger for $[3.4] - [4.6]$. This indicates that the ultra-violet luminosity is dominated by the AGN, rather than star-forming, activity, particularly at high redshift. This is consistent with the argument that star-formation is likely to be suppressed at $Q_{\text{HI}} \gtrsim 10^{56} \text{ sec}^{-1}$ ($L_{\text{UV}} \gtrsim 10^{23} \text{ W Hz}^{-1}$, Curran & Whiting 2012).

(e) Like other studies, we find a correlation between the 21-cm detection rate with $[4.6] - [12]$ colour, although this is only evident at low redshift $z \lesssim 0.1$. There is no strong correlation with the $[3.4] - [4.6]$ colour.

ACKNOWLEDGEMENTS

We wish to thank James Allison, Stas Shabala, Marcin Glowacki and Liz Mahoney for their input. SWD acknowledges receipt of a Victoria Doctoral Scholarship. This research has made use of ASTROPY, a community-developed core Python package for Astronomy (Astropy Collaboration, 2013), the NASA/IPAC Extragalactic Database (NED) which is operated by the Jet Propulsion Laboratory, California Institute of Technology, under contract with the National Aeronautics and Space Administration. This research has also made use of NASA’s Astrophysics Data System Bibliographic Services and ASURV Rev 1.2 (Lavalley et al. 1992), which implements the methods presented in Isobe et al. (1986).

REFERENCES

- Aditya J. N. H. S., Kanekar N., 2018, MNRAS, 473, 59
- Aditya J. N. H. S., Kanekar N., Kurapati S., 2016, MNRAS, 455, 4000
- Aditya J. N. H. S., Kanekar N., Prochaska J. X., Day B., Lynam P., Cruz J., 2017, MNRAS, 465, 5011
- Allison J. R. et al., 2012, MNRAS, 423, 2601
- Allison J. R. et al., 2015, MNRAS, 453, 1249
- Athreya R. M., Kapahi V. K., 1998, JAA&A, 19, 63
- Bahcall J. N., Ekers R. D., 1969, ApJ, 157, 1055
- Carilli C. L., Menten K. M., Reid M. J., Rupen M. P., Yun M. S., 1998, ApJ, 494, 175
- Carilli C. L., Perlman E. S., Stocke J. T., 1992, ApJ, 400, L13
- Carilli C. L., Wang R., van Hoven M. B., Dwarakanath K., Chengalur J. N., Wyithe S., 2007, AJ, 133, 2841
- Chandola Y., Gupta N., Saikia D. J., 2013, MNRAS, 429, 2380
- Chandola Y., Saikia D. J., 2017, MNRAS, 465, 997
- Chandola Y., Sirothia S. K., Saikia D. J., 2011, MNRAS, 418, 1787
- Cluver M. E. et al., 2014, ApJ, 782, 90
- Collier J. D. et al., 2014, MNRAS, 439, 545
- Crighton N. H. M. et al., 2017, in IAU Symposium, Vol. 321, Formation and Evolution of Galaxy Outskirts, Gil de Paz A., Knapen J. H., Lee J. C., eds., pp. 309–314
- Curran S. J., 2012, ApJ, 748, L18
- Curran S. J., 2017a, MNRAS, 470, 3159
- Curran S. J., 2017b, A&A, 606, A56
- Curran S. J., Allison J. R., Glowacki M., Whiting M. T., Sadler E. M., 2013a, MNRAS, 431, 3408
- Curran S. J., Allison J. R., Whiting M. T., Sadler E. M., Combes F., Pracy M. B., Bignell C., Athreya R., 2016a, MNRAS, 457, 3666
- Curran S. J., Duchesne S. W., Divoli A., Allison J. R., 2016b, MNRAS, 462, 4197
- Curran S. J., Hunstead R. W., Johnston H. M., Whiting M. T., Sadler E. M., Allison J. R., Bignell C., 2017a, MNRAS, 470, 4600
- Curran S. J., Reeves S. N., Allison J. R., Sadler E. M., 2016c, MNRAS, 459, 4136
- Curran S. J., Webb J. K., 2006, MNRAS, 371, 356
- Curran S. J., Whiting M. T., 2010, ApJ, 712, 303
- Curran S. J., Whiting M. T., 2012, ApJ, 759, 117
- Curran S. J., Whiting M. T., Allison J. R., Tanna A., Sadler E. M., Athreya R., 2017b, MNRAS, 467, 4514
- Curran S. J. et al., 2011, MNRAS, 416, 2143
- Curran S. J. et al., 2011a, MNRAS, 413, 1165
- Curran S. J., Whiting M. T., Murphy M. T., Webb J. K., Longmore S. N., Pihlström Y. M., Athreya R., Blake C., 2006, MNRAS, 371, 431
- Curran S. J., Whiting M. T., Sadler E. M., Bignell C., 2013b, MNRAS, 428, 2053
- Curran S. J., Whiting M. T., Tanna A., Sadler E. M., Pracy M. B., Athreya R., 2013c, MNRAS, 429, 3402
- Curran S. J., Whiting M. T., Webb J. K., Athreya R., 2011b, MNRAS, 414, L26
- Curran S. J., Whiting M. T., Wiklind T., Webb J. K., Murphy M. T., Purcell C. R., 2008, MNRAS, 391, 765
- De Breuck C. et al., 2003, A&A, 401, 911
- De Breuck C., van Breugel W., Stanford S. A., Röttgering H., Miley G., Stern D., 2002, AJ, 123, 637
- de Waard G. J., Strom R. G., Miley G. K., 1985, A&A, 145, 479
- Donoso E. et al., 2012, ApJ, 748, 80
- Eales S., Rawlings S., Law-Green D., Cotter G., Lacy M., 1997, MNRAS, 291, 593
- Emonts B. H. C. et al., 2013, MNRAS, 430, 3465
- Emonts B. H. C. et al., 2010, MNRAS, 406, 987
- Feigelson E. D., Nelson P. I., 1985, ApJ, 293, 192
- Geréb K., Maccagni F. M., Morganti R., Oosterloo T. A., 2015, A&A, 575, 44
- Geréb K., Morganti R., Oosterloo T. A., 2014, A&A, 569, A35
- Glowacki M. et al., 2017, MNRAS, 467, 2766
- Glowacki M., Allison J. R., Sadler E. M., Moss V. A., Jarrett T. H., 2018, MNRAS, submitted (arXiv:1709.08634)
- Grasha K., Darling J., 2011, in American Astronomical Society Meeting Abstracts, Vol. 43, p. 345.02
- Grasha K., Darling J. K., Bolatto, A. D. Leroy A., Stocke J., 2018, ApJ, submitted
- Gupta N., Salter C. J., Saikia D. J., Ghosh T., Jeyakumar S., 2006, MNRAS, 373, 972
- Hall M., Frank E., Holmes G., Pfahringer B., Reutemann P., Witten I., 2009, SIGKDD Explorations, 11, 10
- Inskip K. J., Tadhunter C. N., Morganti R., Holt J., Ramos Almeida C., Dicken D., 2010, MNRAS, 407, 1739
- Ishwara-Chandra C. H., Dwarakanath K. S., Anantharamaiah K. R., 2003, JAA&A, 24, 37
- Isobe T., Feigelson E., Nelson P., 1986, ApJ, 306, 490
- Jarrett T. H. et al., 2011, ApJ, 735, 112
- Jarvis M. J., Rawlings S., Eales S., Blundell K. M., Bunker A. J., Croft S., McLure R. J., Willott C. J., 2001, MNRAS, 326, 1585
- Kalberla P. M. W., Kerp J., 2009, Ann. Rev. Astr. Ap., 47, 27
- Kanekar N., Prochaska J. X., Ellison S. L., Chengalur J. N., 2009, MNRAS, 396, 385
- Lavalley M. P., Isobe T., Feigelson E. D., 1992, in BAAS, Vol. 24, pp. 839–840
- Lilly S. J., Longair M. S., 1982, in IAU Symposium, Vol. 97, Extragalactic Radio Sources, Heesch D. S., Wade C. M., eds., pp. 413–421
- Maccagni F. M., Morganti R., Oosterloo T. A., Geréb K., Maddox N., 2017, A&A, 604, A43
- Majic R. A. M., 2015, Radio Photometric Redshifts: Estimating radio source redshifts from their spectral energy distributions. Tech. rep., Victoria University of Wellington
- Mirabel I. F., 1989, ApJ, 340, L13
- Moore C. B., Carilli C. L., Menten K. M., 1999, ApJ, 510, L87
- Morganti R., Oosterloo T. A., Tadhunter C. N., van Moorsel G., Killeen N., Wills K. A., 2001, MNRAS, 323, 331
- Morganti R., Sadler E. M., Curran S., 2015, Advancing Astrophysics with the Square Kilometre Array (AASKA14), 134
- Moss V. A. et al., 2017, MNRAS, 471, 2952
- Nagar N. M., Wilson A. S., 1999, ApJ, 516, 97
- Norris R. P. et al., 2011, PASA, 28, 215
- O’Dea C. P., Baum S. A., Gallimore J. F., 1994, ApJ, 436, 669
- Orienti M., Morganti R., Dallacasa D., 2006, A&A, 457, 531
- Osterbrock D. E., 1989, Astrophysics of Gaseous Nebulae and Active Galactic Nuclei. University Science Books, Mill Valley, California
- Ostorero L. et al., 2010, ApJ, 715, 1071
- Ostorero L., Morganti R., Diaferio A., Siemiginowska A., Stawarz Ł., Moderski R., Labiano A., 2017, ApJ, 849, 34
- Page M. J. et al., 2012, Nature, 485, 213
- Peck A. B., Taylor G. B., Conway J. E., 1999, ApJ, 521, 103
- Peck A. B., Taylor G. B., Fassnacht C. D., Readhead A. C. S., Vermeulen R. C., 2000, ApJ, 534, 104

- Pihlström Y. M., Conway J. E., Vermeulen R. C., 2003, *A&A*, 404, 871
- Pihlström Y. M., Vermeulen R. C., Taylor G. B., Conway J. E., 1999, *ApJ*, 525, L13
- Purcell E. M., Field G. B., 1956, *ApJ*, 124, 542
- Rao S. M., Turnshek D. A., Sardane G. M., Monier E. M., 2017, *MNRAS*, 471, 3428
- Reeves S. N., Sadler E. M., Allison J. R., Koribalski B. S., Curran S. J., Pracy M. B., 2015, *MNRAS*, 450, 926
- Röttgering H., de Bruyn G., Pentericci L., Miley G., 1999, in *The Most Distant Radio Galaxies*, Röttgering H. J. A., Best P. N., Lehnert M. D., eds., p. 113
- Salter C. J., Saikia D. J., Minchin R., Ghosh T., Chandola Y., 2010, *ApJ*, 715, L117
- Schlegel D. J., Finkbeiner D. P., Davis M., 1998, *ApJ*, 500, 525
- Shull J. M., Stevans M., Danforth C. W., 2012, *ApJ*, 752, 162
- Skrutskie M. F. et al., 2006, *AJ*, 131, 1163
- Srianand R., Gupta N., Momjian E., Vivek M., 2015, *MNRAS*, 451, 917
- Uson J. M., Bagri D. S., Cornwell T. J., 1991, *PhRvL*, 67, 3328
- van Gorkom J. H., Knapp G. R., Ekers R. D., Ekers D. D., Laing R. A., Polk K. S., 1989, *AJ*, 97, 708
- Vermeulen R. C. et al., 2003, *A&A*, 404, 861
- Willott C. J., Rawlings S., Jarvis M. J., Blundell K. M., 2003, *MNRAS*, 339, 173
- Wolfe A. M., Burbidge G. R., 1975, *ApJ*, 200, 548
- Wright E. L. et al., 2010, *AJ*, 140, 1868
- Yan T., Stocke J. T., Darling J., Hearty F., 2012, *AJ*, 144, 124
- Yan T., Stocke J. T., Darling J., Momjian E., Sharma S., Kanekar N., 2016, *AJ*, 151, 74